Rate Constants for the Reactions of NH_2 and HNO with Atomic Oxygen at Temperatures between 242 and 473 K

Satoshi Inomata and Nobuaki Washida*

Division of Atmospheric Environment, the National Institute for Environmental Studies, 16-2 Onogawa, Tsukuba-shi, Ibaraki, 305-0053 Japan

Received: December 1, 1998; In Final Form: April 28, 1999

A pulsed laser photolysis−discharge flow−photoionization mass spectrometer system has been employed to investigate the kinetics of the reactions $NH_2 + O(^3P)$ (atomic oxygen) and $HNO + O(^3P)$ over the temperature range 242−473 K in 2−7.5 Torr of He. $O(^3P)$ was generated in a microwave discharge of an oxygen−helium mixture, while NH_2 was produced by 193 nm ArF laser photolysis of NH_3. HNO was formed as a reaction product of $NH_2 + O$. Both NH_2 and HNO were photoionized by an Ar resonance lamp and detected as parent ions in a quadrupole mass spectrometer. From the analysis of the time profiles of ion signals for various O-atom concentrations, the overall rate constants are best represented by the pressure and temperature-independent values of $k_1 = (1.2 \pm 0.3) \times 10^{-10}$ and $k_2 = (3.8 \pm 1.3) \times 10^{-11}$ in the units of cm^3 $molecule^{-1}$ s^{-1} for the $NH_2 + O$ and $HNO + O$ reactions, respectively. The value of k_1 is 30−80% larger than values reported previously.

Introduction

Reactions of NH_2 and HNO with atomic oxygen, $O(^3P)$, are important processes governing the yield of NO_x pollutants during the oxidation of ammonia or N-containing fuels.[1,2]

The following three reaction channels have been suggested[3,4] for the reaction of $NH_2 + O(^3P)$:

$$NH_2 + O(^3P) \rightarrow NH + OH \quad \Delta H_{rxn}(298) = -49 \text{ kJ/mol} \tag{1a}$$

$$\rightarrow HNO + H \quad \Delta H_{rxn}(298) = -122 \text{ kJ/mol} \tag{1b}$$

$$\rightarrow H_2 + NO \quad \Delta H_{rxn}(298) = -349 \text{ kJ/mol} \tag{1c}$$

Dransfeld et al.[3] measured the formation of NH and OH radicals in reaction 1 by laser magnetic resonance (LMR) and HNO by laser-induced fluorescence (LIF). They proposed branching ratios of 13 and 87% for paths 1a and 1b, respectively. Adamson et al.[5] measured IR transient absorptions of NH and OH radicals using a tunable infrared laser and proposed that the branching into channel 1a is 5−8%. The overall rate constants for reaction 1 reported recently are $(8.8 \pm 2.5) \times 10^{-11}$ and $(6.5 \pm 1.3) \times 10^{-11}$ cm^3 $molecule^{-1}$ s^{-1} at 296 and 295 K, determined by monitoring the NH_2 decay by LMR[3] and infrared laser absorption,[5] respectively. Measurements of the temperature dependence of the total rate constant for reaction 1 are desirable in order to extend our knowledge of the kinetics of these fast radical−atom reactions.

Two kinetic data[6,7] have been reported for reaction 2. However these rate constants proposed for reaction 2 were obtained by indirect methods.

$$HNO + O(^3P) \rightarrow \text{products} \tag{2}$$

In the present study, the NH_2 radical is produced by pulsed laser photolysis in a discharge flow tube, and HNO is observed as a product of the $O + NH_2$ reaction. Both NH_2 and HNO are detected by a photoionization mass spectrometer, and rate constants were measured under pseudo-first-order condition in NH_2.

Experimental Section

For kinetic experiments, a laser photolysis−discharge flow−photoionization mass spectrometry apparatus was used. Figure 1 displays cross-sectional views of the present apparatus. The apparatus is essentially similar to those used before in this laboratory.[8−11] More abridged schematic diagrams of apparatus have been shown in the previous papers.[8,9] The NH_2 radical produced by pulsed laser photolysis of NH_3 reacted with atomic oxygen in a flow reactor. The inner diameter of the cylindrical Pyrex reactor tube is 13 mm and the length of the reaction zone (from quartz window to pinhole) is 43 cm. Both ends of the reactor are sealed with Suprasil quartz windows in order to transmit the laser beam.

The total and partial pressures of gases were measured with a capacitance pressure gauge (MKS Baratron 170M-35) at a point 88 cm downstream from the pinhole. All pressures reported in this paper are values at the pinhole. The corrections due to the small pressure drop down the reactor tube were determined in separate experiments by measuring the pressure through a movable inlet. This inlet was removed during the photolysis experiments. The concentrations of reagents and flow velocity were determined by a separate calibration of the flow rate as a function of pressure, which includes the modification for pressure drop along the flow reactor. These procedures were carried out at each experimental temperature. The linear flow velocity measured with a bubble meter was 14−33 m s^{-1}, depending upon total presures and temperatures (e.g., 21 m s^{-1} for 4.0 Torr at 295 K).

The reaction zone of the flow reactor was cooled by pumping methyl alcohol that had been chilled in a low-temperature bath/

* To whom correspondence should be addressed.

10.1021/jp984569m CCC: $18.00
Published on Web 06/11/1999

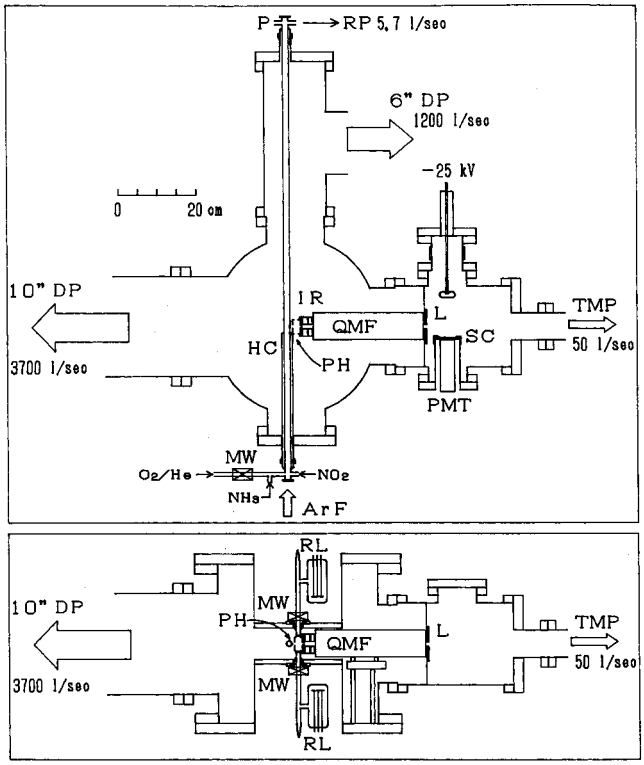

Figure 1. Drawing of the pulsed laser photolysis + discharge flow reactor coupled to the photoionization mass spectrometer. The upper panel is a plane figure and the lower is a side view; P, MKS Baratron pressure gauge; RP, rotary pump; DP, oil diffusion pump; IR, ionization region; L, ion lens; TMP, turbo-molecular pump; QMF, quadrupole mass filter; SC, Al coated plastic scintillator; PH, Pyrex pinhole (ϕ = 0.3 mm); HC, heater or cold jacket; PMT, photomultiplier; RL, rare gas resonance lamp; MW, microwave cavity; ArF, ArF laser (193 nm).

circulator (Thomas TRL-400) through a jacket surrounding the flow reactor tube. Alternatively, the flow reactor tube could be heated with a coiled Nichrome wire. Before each run, the temperature was measured with a copper−constantan thermocouple suspended in the center of inlet tube; these were removed for kinetic experiments. Temperature was uniform within ±2 K.

The oxygen atoms were produced by a microwave discharge (2450 MHz) of a helium−oxygen mixture, resulting in a ratio of oxygen atoms to molecular oxygen of about 0.7. The concentration of oxygen atoms was determined by titrating with an excess of NO_2 according to the reaction $O + NO_2 \rightarrow NO + O_2$ and measuring the NO product using the photoionization mass spectrometer. Then known partial pressures of NO were added to calibrate the instrument sensitivity to NO.

In the present study, the titration with NO_2 to determine oxygen atom concentration was normally done 43 cm upstream from the pinhole. To measure the loss of oxygen atoms on the wall, the titration was carried out at several points in the reaction zone using a movable inlet. The oxygen atom loss was less than 5% between the pinhole and the point of 43 cm upstream when the temperature of the reaction zone was lower than 473 K. Above 473 K, the oxygen atom loss was significant; for example, at 573 K, the loss of oxygen atoms was about 10%. Therefore, in the present study, experiments were carried out at temperatures no greater than 473 K.

Ammonia was mixed with oxygen atoms downstream from the O_2/He discharge. All gas flows were stabilized by a mass flow controller system (UNIT Model UFC-1100). The mixture of NH_3 and $O(^3P)$ in He carrier gas was photolyzed by an ArF-(193 nm) excimer laser (Lambda Physik, LPX120). The resulting NH_2 radical reacted with oxygen atoms. The reacting gas was sampled through a conical Pyrex pinhole (0.3-mm diameter) located in the wall of the tubular Pyrex reactor. A light beam from a microwave-powered discharge lamp passed through the ionization region of a quadrupole mass spectrometer. Both NH_2 and HNO were photoionized by the resonance lines (11.6 and 11.8 eV) from an argon lamp with a LiF window. To enhance the ionizing light, the microwave cavity of the lamp was placed as close as possible (approximately 3 cm) to the ionization region. In this way the detection sensitivity was significantly improved. A typical sensitivity was 1×10^6 counts s^{-1} for a partial pressure of NO of 1 mTorr in the reactor, when it was ionized by an Ar lamp having a LiF window (ionization potential for NO is 9.26 eV). This sensitivity was improved by a factor of 50 over the previous apparatus.[8−10]

The ions formed by photoionization were accelerated and focused into a quadrupole mass filter (Extrel, 4-270-9/150-QC) by several lens elements. After mass selection, the ions were detected by a Daly type electrode (−30 kV), a thin aluminum-coated scintillator, and photomultiplier (Hamamatsu R580). The ion temporal signals were recorded with a LeCroy 9400A digital oscilloscope during a 20 ms period. Signals were transferred to a personal computer after each laser pulse and were discriminated and accumulated for typically 10 000−30 000 laser pulses before analysis. At a repetition rate of 10−15 Hz, the flow velocity was high enough to completely replace the gas in the reaction tube between laser pulses.

The gases NH_3 (Showa Denko, liquid NH_3), O_2 (Nippon Sanso 99.99%), and He (Nippon Sanso 99.9999%) were used as delivered.

Results

1. Detection of Radicals and Molecules. The NH_2 radicals were produced by reaction 3.

$$NH_3 + h\nu\ (193\ \text{nm}) \rightarrow NH_2 + H \qquad (3)$$

A signal at $m/z = 16$ was detected only after the 193 nm laser pulse. The mass spectrum in Figure 2a is the difference spectrum between the signal with irradiation by the photolysis laser and without irradiation. The signal of the parent NH_3^+ ion at $m/z = 17$ appears negative. The signal at $m/z = 16$ is assigned to the NH_2 radical formed by photolysis, because this signal increases with laser irradiation. When a mixture of NH_3 and atomic oxygen was photolyzed, the signal of NH_2^+ decreased as shown in Figure 2b. The only difference between parts b and a of Figure 2 is that the discharge of the O_2/He mixture, upstream of the NH_3 inlet, is on in 2b and off in 2a. Parts c and d of Figure 2 show the mass spectra between m/z = 28.5 and 32.5 in the absence and presence of oxygen atoms, respectively. The formation of HNO via reactions 1 and NO via reaction 2 after reaction 1, as will be described later, are apparent at $m/z = 31$ and 30, respectively. At each point shown in Figure 2, the signal was counted during 4 ms alternatively just before and just after each laser shot, and the difference signal was accumulated for a total of 200 shots at each mass number (10 points per unit mass number).

2. Rate Constant for the $NH_2 + O(^3P)$ Reaction. Parts a and b of Figure 3 show the time profiles of the NH_2^+ signal at 295 K when NH_3 was photolyzed in the absence and in the presence of oxygen atoms, respectively. The absorption cross section of NH_3 at 193 nm is reported to be 9.3×10^{-18} cm^2 $molecule^{-1}$ at 300 K.[12,13] The concentrations of NH_3 used in

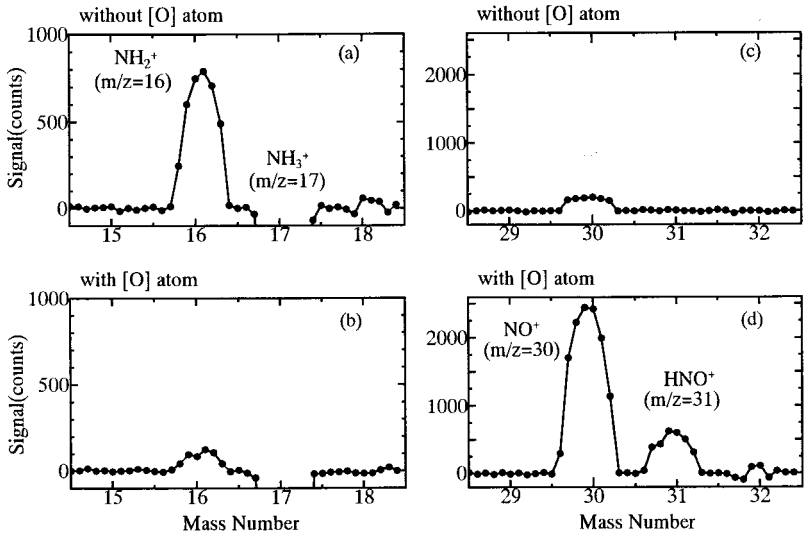

Figure 2. Mass spectra of the ion signal observed in the $NH_3 + O(^3P) + h\nu$ (193 nm) system. The mass spectra shown are the difference spectra between the signal with irradiation by the laser (193 nm) and without irradiation. The signal was 200 shots accumulated alternatively with and without laser at each mass number (dot). Conditions: $T = 295$K, $P = 4$Torr (buffer gas, He), $[NH_3] = 2.0 \times 10^{13}$ molecules cm^{-3}, ArF laser fluorescence $= 1.6 \times 10^{15}$ photon cm^{-2}, (a) $[O] = 0$ (O_2/He discharge off), (b) $[O] = 5.8 \times 10^{12}$ molecules cm^{-3} (O_2/He discharge on), (c) $[O] = 0$, (d) $[O] = 5.8 \times 10^{12}$ molecules cm^{-3}.

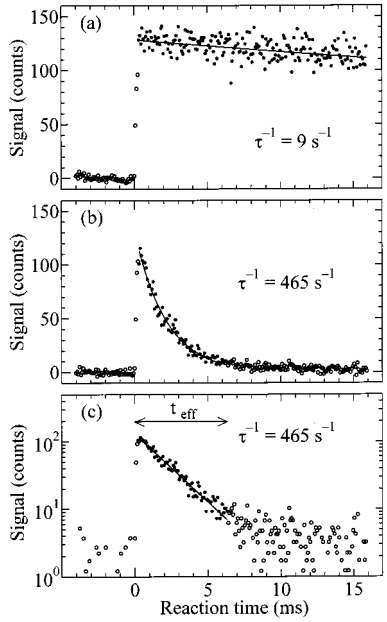

Figure 3. Typical temporal profile of NH_2^+ at 295K: (a) in the absence of O; (b) and (c) $[O]_0 = 4.09 \times 10^{12}$ molecule cm^{-3}, $[NH_2]_0 = 1 \times 10^{11}$ molecule cm^{-3}, total pressure (mostly He) $= 4$ Torr. Solid lines through the data are the exponential function (eq 4) fitted to solid circles by a least-squares method. (c) A logarithmic plot of the data from b. "t_{eff}" means the effective reaction time used to determine the value of k'.

the present study were $(2.5-8.5) \times 10^{12}$ molecule cm^{-3}, and the laser power was 1.4−2.7 mJ cm^{-2} pulse^{-1}. Therefore, less than 5% of the laser light was absorbed by NH_3 in the reaction region, and the NH_2 concentration should be in the range of $(5-12) \times 10^{10}$ molecule cm^{-3}.

The decay shown in Figure 3b reflects the decrease of NH_2 by reaction 1. If there are no effective side reactions, such as radical−radical reactions, and no significant change of the initial concentration of oxygen atoms, $[O]_0$, the time dependence should be given by a single-exponential function:

$$[NH_2] = [NH_2]_0 \exp(-k't) \tag{4}$$

Here, $[NH_2]_0$ stands for the initial NH_2 radical concentration and k' stands for the decay rate of the NH_2 radical written as

$$k' = k_1[O]_0 + k_w \tag{5}$$

where k_1 is the overall rate constant for reaction 1, and k_w represents other loss processes (loss on the walls and reactions with parent molecules or with impurities), which are responsible for the decay shown in Figure 3a (9 s^{-1}). The values of k' were determined by logarithmic fitting the decay of NH_2^+ to eq 4, as shown in Figure 3c. The solid circles in Figure 3 show the data points used to determine the value of k'. The reaction time corresponding to the solid circles is defined as "effective reaction time (t_{eff})".

In the present study, the initial concentrations of NH_2, should be low enough to prevent radical−radical reactions from affecting the decay of NH_2. To estimate these effects, kinetic modeling was performed. The relevant reactions as well as their Arrhenius parameters are presented in Table 1. The initial conditions used to model the system were set to be the same as the experimental ones. The modeling results show that the NH_2 radical is consumed exponentially until its concentration decreases to 2% of $[NH_2]_0$, even at 473 K. And during this reaction time, corresponding to "t_{eff}", reaction 1 is the dominant process consuming NH_2; the contributions by other reactions are less than 1% of those by reaction 1.

On the other hand, the initial concentrations of the oxygen atoms, $[O]_0 = (1-6) \times 10^{12}$ molecule cm^{-3}, could be changing during the NH_2 decay. The initial concentration of oxygen atoms, $[O]_0$, was determined by the NO_2 titration at 43 cm upstream of the pinhole as described before. At high temperature, NH_3 can react with the $O(^3P)$ directly, although the reaction is slightly endothermic.

$$NH_3 + O(^3P) \rightarrow NH_2 + OH \quad \Delta H_{rxn}(298) = +26.3\text{kJ/mol} \tag{6}$$

The recommended rate constant[14] for reaction 6 is 1.6×10^{-11} exp $(-3670/T)$ cm^3 molecule^{-1} s^{-1}. Modeling shows that the consumption of oxygen atoms by reaction 6 and subsequent

TABLE 1: Reactions and Rate Constants[a] Used in the Modeling.

reaction	$\Delta H_{rxn}(298)$[b]	A[c]	B	E/R	ref
$O + NH_3 \rightarrow NH_2 + OH$	+26	1.6E(−11)[d]	0.0	3670	14
$O + NH_2 \rightarrow HNO + H$	−122	1.1E(−10)	0.0	0	3, this work
$O + NH_2 \rightarrow NH + OH$	−49	1.2E(−11)	0.0	0	5, this work
$O + HNO \rightarrow OH + NO$	−220	3.8E(−11)	0.0	0	this work
$O + OH \rightarrow H + O_2$	−70	2.2E(−11)	0.0	−120	15
$O + NH \rightarrow H + NO$	−293	1.5E(−10)	0.0	0	14
$OH + NH_3 \rightarrow NH_2 + H_2O$	−44	1.7E(−12)	0.0	710	15
$OH + NH_2 \rightarrow O + NH_3$	−26	3.3E(−14)	0.405	250	14
$OH + NH \rightarrow N + H_2O$	−185	8.3E(−13)	0.5	1000	16
$OH+NH \rightarrow HNO + H$	−98	8.3E(−13)	0.5	1000	16
$OH + HNO \rightarrow H_2O + NO$	−290	1.8E(−11)	0.0	0	16
$OH + OH \rightarrow H_2O + O$	−71	4.2E(−12)	0.0	240	15
$H + NH_2 \rightarrow H_2 + NH$	−56	6.7E(−11)	0.0	1840	16
$H + NH \rightarrow H_2 + N$	−97	1.7E(−11)	0.0	0	14
$H + HNO \rightarrow H_2 + NO$	−227	7.5E(−13)	0.72	327	16
$NH + NO \rightarrow N_2O + H$	−142	3.8E(−11)	0.0	0	17
$NH + NO \rightarrow N_2 + OH$	−403	9.4E(−12)	0.0	0	17
$NH + O_2 \rightarrow NO + OH$	−223	9.0E(−15)	0.0	0	18
$NH_2 + NO \rightarrow N_2 + H_2O$	−522	3.8E(−12)	0.0	−450	15
$N + OH \rightarrow NO + H$	−203	4.7E(−11)	0.0	0	14
$N + NO \rightarrow N_2 + O$	−314	2.1E(−11)	0.0	−100	15

[a] The tabulated rate constants are defined by $k = AT^B \exp(-E/RT)$ and rate constants are in units of cm^3 molecule^{-1} s^{-1}. [b] $\Delta H_{rxn}(298)$ is in units of kJ/mol. [c] A is in units of cm^3 molecule^{-1} s^{-1}. [d] Read as, for example, 1.6×10^{-11} cm^3 molecule^{-1} s^{-1}.

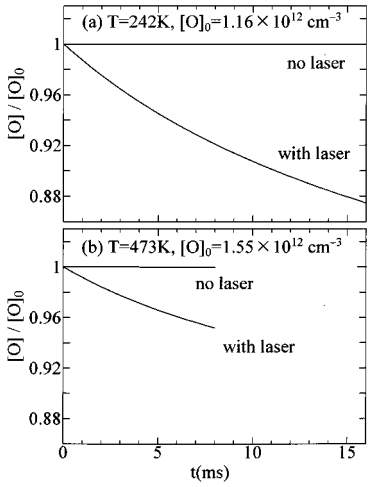

Figure 4. Kinetic modeling of temporal concentration profiles for oxygen atoms for the following initial conditions: (a) [total] = 1.6×10^{17}, $[NH_3]_0 = 8.1 \times 10^{12}$, $[NH_2]_0 = 1 \times 10^{11}$, $[O]_0 = 1.16 \times 10^{12}$, $T = 242$ K; (b) [total pressure] = 8.5×10^{16}, $[NH_3]_0 = 4.2 \times 10^{12}$, $[NH_2]_0 = 7.2 \times 10^{10}$, $[O]_0 = 1.55 \times 10^{12}$, $T = 473$K; all are in units of molecule cm^{-3}. Values of t_{eff} are 8 ms in both cases. Results of "no laser" and "with laser" show the decay of oxygen atoms caused by reactions 1 and 6 and the subsequent radical−atom reactions.

radical−atom reactions is very small even at 473 K (less than 0.1% of the initial oxygen-atom concentration (see Figure 4 "no laser").

When the NH_3 is photolyzed, oxygen atoms are consumed more by reaction 1 and the subsequent reactions shown in Table 1. Figure 4 shows two examples of the model calculation on the decay of oxygen atoms. The loss of oxygen atoms is larger for low temperature (Figure 4a). This is caused mostly by the negative temperature effect in reaction 7.

$$O + OH \rightarrow H + O_2 \qquad (7)$$

As shown in Figure 4, the consumption of oxygen atoms during the effective reaction time (t_{eff}) is less than 10%.

To evaluate the effect of the oxygen-atom consumption on the determination of the rate constant, the average oxygen-atom concentrations, $[\bar{O}]$, during the effective reaction time were calculated by eq 8.

$$[\bar{O}] = \frac{1}{t_{eff}} \int_0^{t_{eff}} [O]\, dt \qquad (8)$$

Where [O] is the oxygen-atom concentration obtained from the model calculation (Figure 4 "with laser").

The values of k' were determined for various O-atom concentrations by fitting the decay profiles of NH_2^+ to eq 4. Results of a case at 242 K (including the oxygen-atom decay shown in Figure 4a) are compiled in Table 2. The value of k_1 was obtained from the slope of the plot of k' against the O-atom concentration according to eq 5. Plots of k' vs $[\bar{O}]$ and $[O]_0$ are shown in Parts a and b of Figure 5 and slopes give the values of k_1 to be $(1.46 \pm 0.25) \times 10^{-10}$ and $(1.43 \pm 0.25) \times 10^{-10}$ cm^3 molecule^{-1} s^{-1}. Indicated error limits represent the 95% confidence limits of the least-squares fitting of the plots. The difference of the two results is at most 2%. $[\bar{O}]$ was used to analyzing all of the rate data in the present study.

The measurements were carried out under various total pressures, initial radical concentrations, laser powers, and four different temperatures. The results are summarized in Table 3. No total pressure dependence was observed for k_1 between 2.2 and 7.5 Torr of He (Figure 6a). The log of the measured values of k_1 are plotted in Figure 6b against the reciprocal of the absolute temperature. The dashed line in Figure 6b is a linear least-squares which shows a slight negative activation energy, $E_a = -570 \pm 920$ J/mol. The small reactive activation energy is not significant considering the 95% confidence limits. It is concluded that there is no significant variation of k_1 with temperature between 242 and 473 K within experimental error. The best representation for k_1 is just the average (unweighted) of all measured values,

$$k_1 = (1.2 \pm 0.3) \times 10^{-10}\ cm^3\ molecule^{-1}\ s^{-1} \quad (T = 242-473\ K) \qquad (9)$$

where the indicated error was chosen to overlap all of the determinations in this temperature range.

TABLE 2: Observed Decay Rate of NH_2 and Oxygen-Atom Concentration at 242 K

total pressure $\times 10^{-17}$ [a]	laser power (mJ/cm^2)	$[NH_3]_0 \times 10^{-12}$ [a]	$[NH_2]_0 \times 10^{-10}$ [a]	$[O]_0 \times 10^{-12}$ [a]	t_{eff} (ms)	$[\bar{O}] \times 10^{-12}$ [a]	k' (s^{-1})
1.64	1.5	6.4	8.7	0	16.0	0	17 ± 6
1.62	1.5	8.1	11.0	1.16	8.0	1.11	160 ± 22
1.63	1.5	7.7	10.5	1.56	8.0	1.50	209 ± 29
1.60	1.4	6.4	8.1	2.39	6.4	2.33	330 ± 38
1.65	1.5	7.1	9.6	2.95	7.2	2.87	397 ± 42
1.63	1.5	7.7	10.5	3.27	6.4	3.18	434 ± 44
1.62	1.5	8.4	11.4	3.75	4.0	3.67	588 ± 80

[a] Unit is molecule cm^{-3}.

TABLE 3: Rate Constants for $NH_2 + O(^3P)$

temp (K)	total pressure $\times 10^{-17}$ [a]	laser power (mJ/cm^2)	$[NH_3]_0 \times 10^{-12}$ [a]	$[NH_2]_0 \times 10^{-10}$ [a]	$[\bar{O}] \times 10^{-12}$ [a]	$k_1 \times 10^{10}$ [b]
242	1.6	1.4−1.5	6.4−8.4	8.1−11.4	0−3.75	1.43 ± 0.25
295	1.3	1.7−2.2	4.7−6.0	7.2−11.9	0−5.20	1.07 ± 0.14
295	2.4	1.8−2.0	2.6−4.7	4.5−8.1	0−4.52	1.31 ± 0.27
295	0.7	1.7	5.7−8.4	8.8−12.9	0−4.35	1.27 ± 0.23
344	1.1	1.6−1.7	4.1−6.3	6.3−9.7	0−4.21	1.28 ± 0.34
344	1.5	1.5−1.6	4.3−5.9	5.8−8.4	0−5.89	1.15 ± 0.16
473	0.8	1.9−2.1	4.2−6.2	7.2−11.2	0−5.39	1.17 ± 0.11
473	0.7	1.6−2.3	3.0−4.8	5.4−10.0	0−5.80	1.19 ± 0.20

[a] Unit is molecule cm^{-3}. [b] Unit is cm^3 molecule^{-1} s^{-1}.

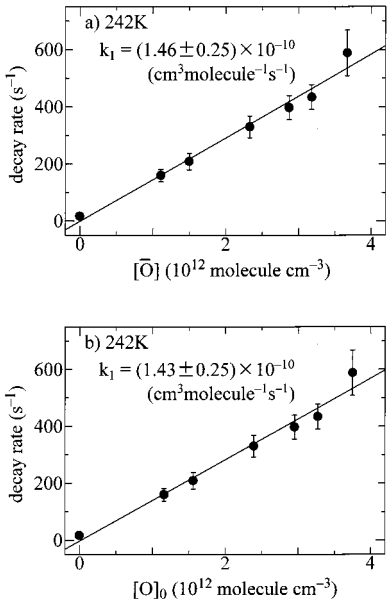

Figure 5. Plot of the decay rate of NH_2^+ against (a) [$\bar{O}$] and (b) $[O]_0$. The experimental conditions are shown in Table 2.

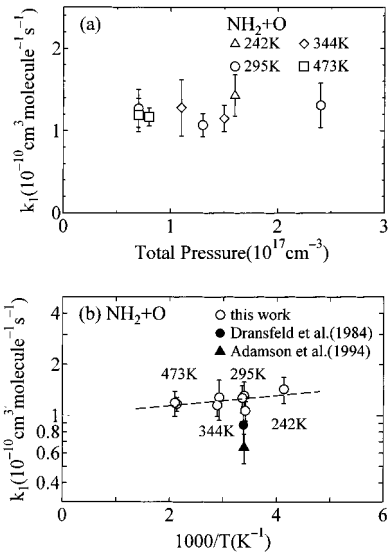

Figure 6. Pressure and temperature dependence of the rate constants for reaction $NH_2 + O$: (a) pressure dependence; (b) Arrhenius plot of (open symbols) this work, (●) Dransfeld et al. (ref 3), (▲) Adamson et al. (ref 5). The dashed line drawn is obtained by the linear least-squares fit of the open symbols.

In Figure 6b, values for k_1 reported by Dransfeld et al.[3] and Adamson et al.[5] are plotted as filled symbols. The rate constant for the reaction of $NH_2 + O$ obtained in the present study is 30−80% larger than those reported previously.

3. Rate Constant for the HNO + O(^{3}P) Reaction. As shown in Figure 2, both HNO and NO were formed when NH_2 radicals reacted with atomic oxygen. Time profiles of signals of HNO^+ ($m/z = 31$) and NO^+ ($m/z = 30$) are shown in Figure 7 together with the signal of NH_2^+ ($m/z = 16$). The slight delay of the rise in the NH_2^+ signals in Figure 7a is caused by the pinhole sampling (the diameter of laser light beam is smaller than that of reaction tube). As shown in Figure 7, the signal of HNO^+ rises, corresponding to the decrease of the NH_2^+. Solid lines through the data are obtained from the kinetic modeling using the rate data compiled in Table 1. This means that HNO radicals are produced by reaction 1b and that the rate for reaction 2 (k_2) could be obtained by double exponential fit to eq 10.

$$[HNO] = A\{\exp(-k_1[\bar{O}]t) - \exp(-k''t)\} \qquad (10)$$

Here, A is a constant and k'' stands for the decay rate of the HNO written as

$$k'' = k_2[\bar{O}] + k'_w \qquad (11)$$

where k_2 is the overall rate constant for reaction 2 and k'_w represents other loss processes. A least-squares fitting of the HNO signal to the double exponential eq 10 is shown by a dashed line in Figure 7b, which is overlapping with a solid line. Where the value shown by eq 9 was used for the k_1 value. In this case, the value for $k_1[\bar{O}]$ is 882 s^{-1}.

The value of k_2 was obtained from the slope of the plot of k'' against the O-atom concentration according to eq 11, which is the same procedure as described in the case of NH_2. One of the typical plots of k'' vs [$\bar{O}$] is shown in Figure 8. In this case the slope gives a value of k_2 to be $(3.35 \pm 0.71) \times 10^{-11}$ cm^3 molecule^{-1} s^{-1}. The measurements were carried out under various total pressures and four different temperatures. All results of rate measurements are summarized in Table 4.

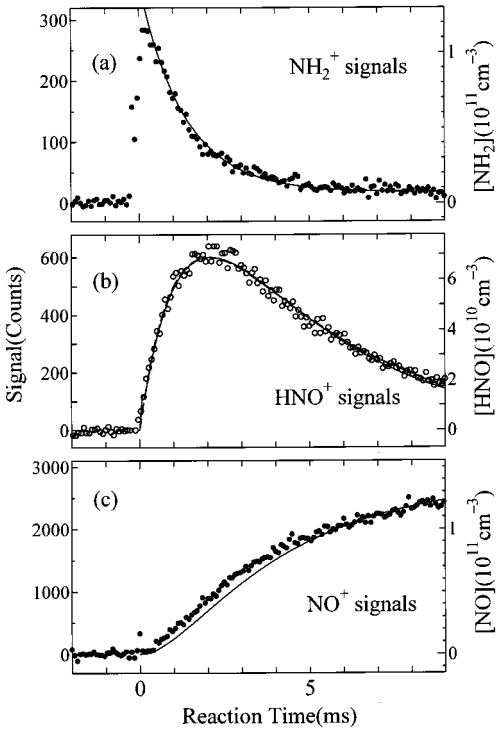

Figure 7. Time profiles of NH_2^+, HNO^+, and NO^+ at 295 K. Conditions: $[NH_3]_0 = 7.8 \times 10^{12}$, $[O]_0 = 7.6 \times 10^{12}$, in units of molecule cm^{-3}. Solid lines through the data were calculated by modeling. For the dashed line in b, see the text.

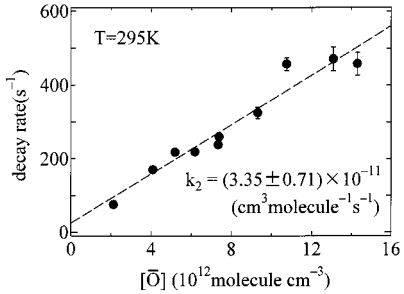

Figure 8. Typical plot of the decay rate of HNO^+ against O-atom concentration. The experimental conditions are shown in the third line in Table 4.

Figure 9a,b shows the pressure and temperature dependence of k_2. No pressure dependence was observed between 2.2 and 7.5 Torr of buffer gas (mostly He). A linear least-squares treatment of the values in Figure 9b (dashed line) gives a small positive activation energy, $E_a = 1240 \pm 1130$ J/mol, but the 95% confidence limits show that there is only marginal significance for this value. It is perhaps better to represent k_2 as temperature independent,

$$k_2 = (3.8 \pm 1.3) \times 10^{-11}\ \text{cm}^3\ \text{molecule}^{-1}\ \text{s}^{-1} \quad (T = 242-473\ \text{K}) \quad (12)$$

where the error is chosen to overlap all the determinations.

As can be seen in Figure 7c, the NO molecule was formed as the HNO was consumed, but it was not produced during the initial loss of NH_2. These results suggest that the NO is produced by reaction 2a and that reaction 1c is not a major reaction channel even through 1c is the most exothermic path.

$$HNO + O(^3P) \rightarrow OH + NO \quad \Delta H_{rxn}(298) = -220\ \text{kJ/mol} \quad (2a)$$

The kinetic model fitting of the time profile of NO^+ using the rate data in Table 1 is shown by a solid line in Figure 7c. Since the experimental data do not coincide with the solid line during the short reaction time, some production of NO in reaction 1 is required; the branching ratio of reaction 1c is estimated to be 10−20% of that of reaction 1.

Discussion

1. Photoionization of NH_2 and HNO. The detection of NH_2[19] and HNO[8] by the photoionization has been reported previously. The ionization potential (IP) of the NH_2 radical is reported to be 11.46 ± 0.01 and 11.4 ± 0.1 eV, as measured by photoelectron spectroscopy[20] and electron impact mass spectrometry.[21] The reported ionization potential for DNO is 10.29 ± 0.14 eV.[22] Recently several values for the heat of formation of HNO have been reported: 102.5,[23] 111.8 ± 3.3,[24] and 110.02 ± 0.25[25] kJ/mol. The heat of formation of HNO^+ has been reported[26] to be 1075.0 ± 5.9 kJ/mol, which is determined from the photodissociative ionization reactions of hydroxylamine. From the above values, the IP of HNO can be calculated to be 10.0−10.1 eV. These values for NH_2 and HNO are consistent with the results in the present study, in that NH_2 and HNO were both photoionized by the argon resonance lines (11.6 and 11.8 eV). From the observed signal-to-noise ratio, the detection limits of NH_2 and HNO were estimated to be about 3×10^9 and 2×10^9 molecule cm^{-3}, respectively.

2. Effect of the Vibrationally Excited NH_2. The rate constant for the reaction of $NH_2 + O$ obtained in the present study is 30−80% larger than those reported in previous studies.[3,5] Since in the present study the NH_2 radical was produced by the photodecomposition of NH_3, it is possible that the NH_2 radicals formed are excited vibrationally. To examine whether the measured rate constants are affected by vibrationally excited NH_2, the laser-induced fluorescence (LIF) spectrum of NH_2 was measured.

Figure 10 shows the LIF spectra of NH_2 when NH_3 was photolyzed by an ArF (193 nm) excimer laser at 2 Torr of total pressure (mostly He). Figure 10a shows the LIF excitation spectrum of the NH_2 radical measured just after the laser photolysis (60 μs). Many hot bands are apparent, although the assignment of bands is difficult. On the other band, as shown in Figure 10b, all bands can be assigned to be transitions from $v'' = 0$ when the spectrum was measured 1 ms after photolysis the laser shot. Spectral assignment shown in Figure 10b was carried out according to the absorption spectra of NH_2 reported by Ross et al.[27] These results show that 1 ms is a sufficient delay time for the hot NH_2 to be relaxed completely at 2 Torr of He buffer gas.

In the present study, the measurements of the rate for the $NH_2 + O$ reaction were carried out 1−8 ms after the photolysis laser shot with 2−7.5 Torr of He buffer gas. Therefore, the rate constants obtained in the present study are not affected by the vibrationally excited NH_2.

It has been reported[28] that 193 nm photolysis of NH_3 prepares $NH_2(\tilde{A}^2A_1)$ but the quantum yield for the formation of $NH_2(\tilde{A}^2A_1)$ is very small (2.5%) and that an average radiative lifetime is 31 μs. Therefore, the $NH_2(\tilde{A}^2A_1)$ formed by the 193 nm photolysis of NH_3 does not perturb the spectra shown in Figure 10 and also the rate measurements in the present study.

3. Comparison with Previous Studies. The rate coefficient for the reaction of $NH_2 + O$ at room temperature has been measured by Dransfeld et al.[3] and Adamson et al.[5] The methods, conditions, and results of these measurements are summarized in Table 5 along with the results of the present study. Dransfeld

TABLE 4: Rate Constants for HNO + O(^{3}P)

temp (K)	total pressure × 10^{-17} [a]	laser power (mJ/cm^2)	$[NH_3]_0 \times 10^{-12}$ [a]	$[NH_2]_0 \times 10^{-10}$ [a]	$[\bar{O}] \times 10^{-12}$ [a]	$k_2 \times 10^{11}$ [b]
242	1.7	1.4−1.5	6.3−7.6	8.1−10.3	2.39−17.03	3.50 ± 0.55
242	2.1	1.4−1.6	5.9−7.9	8.5−10.3	5.54−17.51	3.93 ± 1.27
295	1.3	1.7−2.2	4.7−6.0	7.2−11.9	2.13−14.53	3.35 ± 0.71
295	2.4	1.7−1.8	3.0−5.2	4.9−8.5	2.32−14.56	3.24 ± 0.97
295	0.7	1.7−1.8	5.6−6.8	9.1−10.9	1.96−13.45	3.18 ± 0.79
344	1.5	1.5−1.7	4.2−6.4	5.8−9.8	3.03−13.44	3.60 ± 0.31
344	1.2	1.3−1.7	4.1−7.2	5.7−8.5	3.56−15.49	3.79 ± 0.53
473	0.9	1.9−2.4	4.3−5.8	7.8−11.7	3.41−12.61	5.03 ± 0.94
473	0.8	1.6−2.0	3.5−5.4	5.7−9.8	5.35−13.67	4.60 ± 0.97

[a] Unit is molecule cm^{-3}. [b] Unit is cm^3 molecule^{-1} s^{-1}.

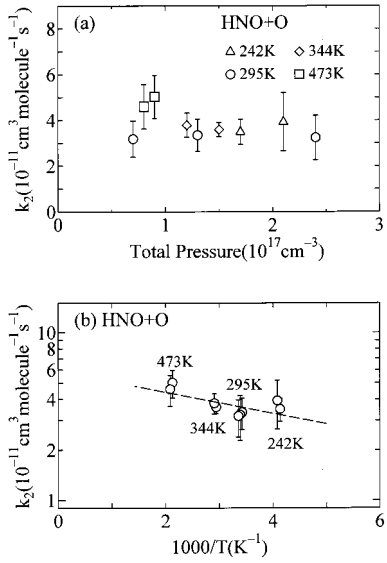

Figure 9. Pressure and temperature dependence of the rate constants for reaction HNO + O: (a) pressure dependence and (b) Arrhenius plot. The dashed line drawn is obtained by the linear least-squares fit.

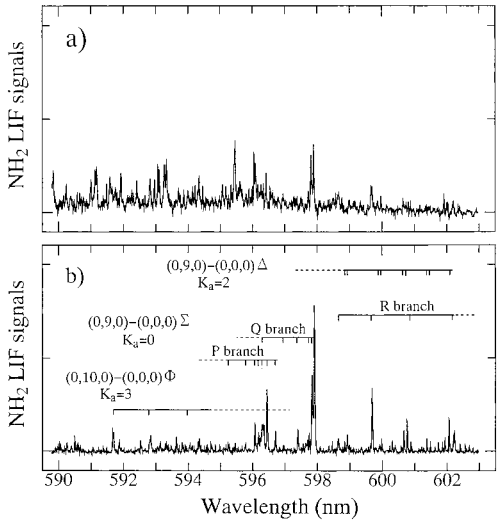

Figure 10. The LIF spectra of NH_2 in the region 590−603 nm when NH_3 was photolyzed by an ArF*(193 nm) excimer laser under 2 Torr of total pressure (mostly He): (a) the LIF spectrum of NH_2 just after the photolysis laser shot (60 μs) and (b) the LIF spectrum measured 1 ms after photolysis laser shot.

et al.[3] produced NH_2 radicals by reacting F-atoms with NH_3 in a discharge flow tube, and the NH_2 radical reacted with excess O-atoms generated in a microwave discharge of O_2 in He. Time profiles of NH_2 (also O, OH, and NH) were measured with the LMR and LMR/ESR spectrometers. Absolute O-atom concentration was determined using the titration reaction O + NO_2 → O_2 + NO. From the slope of the decay rates of NH_2 vs [O], they proposed the value of $(8.8 \pm 2.5) \times 10^{-11}$ cm^3 molecule^{-1} s^{-1} for k_1.

Adamson et al.[5] produced NH_2 radicals by ArF excimer laser (193 nm) photolysis of NH_3. The NH_2 radical was reacted with O-atoms, and time profiles of NH_2 (also NH and OH) were monitored by IR absorption using a tunable infrared colorcenter laser. From the slope of the decay constants for NH_2 plotted against O-atom concentration, the rate constant for the overall reaction of NH_2 with O was determined as $(6.5 \pm 1.3) \times 10^{-11}$ cm^3 molecule^{-1} s^{-1}.

As shown in Table 5, previous procedures used to determine k_1 were not much different from the present ones, except for the method used to follow the NH_2 radical (also, the NO measurement after O-atom titration). The most critical measurement for determing k_1 is an accurate determination of the O-atom concentration, including an estimate of the decay of oxygen atoms during the reaction. Larger values for the $[O]_0/[NH_2]_0$ ratio are desirable, although in each study the O-atom decay was estimated by modeling.

In the studies by Dransfeld et al.,[3] some of the measurements were carried out with small $[O]_0/[NH_2]_0$ ratios. However, they directly measured the time profiles of O-atom signals by LMR. Consequently, the average O-concentration, $[\bar{O}]$, was used to determine the rate constant. The reason for the difference between the results by Dransfeld et al.[3] and those in the present study is not clear. However, the rate constant of $(9-15) \times 10^{-11}$ cm^3 molecule^{-1} s^{-1} (considering the stated errors) obtained in the present study overlaps the range of $(6.3-11.3) \times 10^{-11}$ cm^3 molecule^{-1} s^{-1} reported by Dransfeld et al.[3]

In the studies by Adamson et al.,[5] measurements were carried out under very high NH_2 and O-atom concentrations. It is possible that their ratio of $[O]_0$ to $[NH_2]_0$ was not large enough for a reliable determination of the rate constant.

4. Reaction Rate and Mechanism of the NH_2 + O Reaction. The value for k_1 obtained in the present study shows that the reaction of the NH_2 radical with an oxygen atom is very fast, about half the collision frequency. Such fast reactions have been reported in other radical−atom reactions such as CH_3 + O,[29,30] HCO + O,[31] and H + HCO.[32] In addition, almost no activation energy has been observed for these fast reactions.[29,30,32] The reaction of NH_2 + O appears to be similar.

In the previous studies[3] of reaction 1, the dominant reaction path (87%) was proposed to be reaction 1b, HNO + H, which is thought to be an addition reaction. The second proposed reaction path, reaction 1a producing NH + OH (5−13%), is likely to be an abstraction reaction.[3,5] Recently, Yang et al.[33] performed ab initio theoretical calculations of the ground (^{2}A″) and excited (^{4}A′) surfaces for the reaction of NH_2 with O. Their calculated results suggest that the direct hydrogen atom abstraction reaction to produce NH + OH, which proceeds on the ^{4}A′ surface, would be expected to have an activation energy, because

TABLE 5: Summary of the Measurements of the Rate Constant for the Reaction of NH_2 + O at Room Temperature

red	NH_2 source (NH_2 monitor)	O-atom source (Titration method)	total pressure, Torr (buffer gas)	i.d. of reactor, mm (flow rate, m/s)	$[NH_2]_0 \times 10^{-11}$, molecule cm^3	$[O]_0 \times 10^{-12}$, molecule cm^{-3}	$[O]_0/[NH_2]_0$	reaction time, ms	k_1 at room temperature $\times 10^{11}$, cm^3 $molecule^{-1}$ s^{-1}
Dransfeld et al.[3]	NH_3 + F (LMR)[a]	O_2/He discharge (O + NO_2)	1.4−2.5 (He)	10 (16−50)	0.17−19	0.43−6.0	1.4−255	5−20	8.8 ± 2.5
Adamson et al.[5]	NH_3 + hν (193 mm) (IR absorption)	O_2/He discharge (O + NO_2)	2.3−3.3 (He + CH_4)	54 (0.6)	500−1000	300−800	<8	0.01−0.1	6.5 ± 1.3
this work	NH_3 + hν (193 mm) (PIMS)	O_2/He discharge (O + NO_2)	2−7.5 (He)	13 (13−33)	0.5−1.2	1−6	10−100	1−8	12 ± 3

[a] LMR = laser magnetic resonance. [b] PIMS = photoionization mass spectrometry.

the transition state is 28 kJ/mol above the energy of the separated NH_2 + O reactants. According to their calculation, the three reaction paths 1a, 1b, and 1c proceed on the $^2A''$ surface through an H_2NO intermediate which lies 367 kJ/mol below the separated NH_2 + O reactants. This intermediate may either fragment to form H + HNO or H_2 + NO, or undergo a 1,2-hydrogen shift to form *trans*-HNOH. This second intermediate may dissociate to either NH + OH or H + HNO, or isomerize to *cis*-HNOH which, in turn, may dissociate into the same products.

$$\begin{aligned} NH_2 + O \rightarrow H_2NO \rightarrow\ & H + HNO \\ \rightarrow\ & (TS) \rightarrow H_2 + NO \\ \rightarrow\ & (TS) \rightarrow \textit{trans}\text{-}HNOH \rightarrow NH + OH \\ \rightarrow\ & (TS) \rightarrow H + HNO \\ \rightarrow\ & (TS) \rightarrow \textit{cis}\text{-}HNOH \rightarrow NH + OH \\ \rightarrow\ & (TS) \rightarrow H + HNO \end{aligned} \qquad (13)$$

Their calculations show that the energies of the three transition states (TS) are below the energy of the separated NH_2 + O reactants. Consequently, all of these reaction paths proceed through an addition reaction. The absence of a significant activation energy in reaction 1 as obtained in the present study is in agreement with the results of the theoretical calculation. However, the reason reaction 1b is dominant, and reaction 1c is minor, cannot be explained at the present time.

5. Reaction Rate and Mechanisms of the HNO + O Reaction. Two kinetic data[6,7] have been reported for reaction 2. Campbell and Handy[6] measured the rate constant for reaction 2 under the O + H_2 + NO system and reported a value of 1.6×10^{-11} cm^3 $molecule^{-1}$ s^{-1} as a lower limit at 425 K. Tsang and Herron[7] proposed a value of 6×10^{-11} cm^3 $molecule^{-1}$ s^{-1} over the temperature range from 300 to 2500 K. The value was estimated on the assumption that reaction 2 is analogous to the O + HO_2 reaction. Therefore, the value for k_2 of $(3.8 \pm 1.3) \times 10^{-11}$ cm^3 $molecule^{-1}$ s^{-1} was first obtained by a direct measurement in the present study.

The rate constant for reaction 2 is about half of that for reaction 1. The reaction of HNO + O is similar to reactions O + NO_2 and O + HO_2, for which rate constants[15] are 6.5×10^{-12} $\exp[(120 \pm 120)/T]$ and 3×10^{-11} $\exp[(200 \pm 100)/T]$ cm^3 $molecule^{-1}$ s^{-1}, respectively.

$$NO_2 + O \rightarrow NO + O_2 \qquad (14)$$

$$HO_2 + O \rightarrow OH + O_2 \qquad (15)$$

These two reactions have been suggested to be addition reactions through NO_3[34,35] and HO_3[36,37] intermediates. The value of the rate constant for reaction 2 is close to that for reaction 15.

Four reaction paths are energetically possible for the HNO + O reaction:

$$HNO + O(^3P) \rightarrow OH + NO \quad \Delta H_{rxn} = -220 \text{ kJ/mol} \qquad (2a)$$

$$\rightarrow H + NO_2 \quad \Delta H_{rxn} = -98 \text{ kJ/mol} \qquad (2b)$$

$$\rightarrow NH + O_2 \quad \Delta H_{rxn} = -3 \text{ kJ/mol} \qquad (2c)$$

$$\xrightarrow{M} HONO \quad \Delta H_{rxn} = -329 \text{ kJ/mol} \qquad (2d)$$

Among these four processes, the three-body reaction 2d can be omitted because no pressure dependence was observed in reaction 2. Reaction 2c is not important because it is almost thermoneutral. Since no NO_2 was observed in the present study, reaction 2b is not a significant pathway, even though the rate for reaction 14 is slow enough that the rise of an NO_2^+ signal could have been seen. Therefore, reaction 2a appears to be the major route for reaction 2. This result is strongly supported by the observed rise of the NO^+ signal the HNO signal decay (Figure 7).

It is interesting to compare reaction 2a with the isomeric H + NO_2.

$$H + NO_2 \rightarrow OH + NO \quad \Delta H_{rxn}(298) = -122 \text{ kJ/mol} \qquad (16)$$

Reaction 16 is known to be very fast with a rate constant of 2.2×10^{-10} $\exp(-182/T)$ cm^3 $molecule^{-1}$ s^{-1}.[38] This reaction is known[39−43] to produce vibrationally excited OH radicals, and most of the available energy is used to vibrationally excite the OH (up to $v'' = 3$). The reaction mechanism has been explained as an abstraction reaction through an HONO intermediate.[41,42] In the case of reaction 2a, two reaction mechanisms, i.e., an abstraction through an OHNO complex and an addition reaction forming an HNO_2 intermediate, can be considered. After formation of the intermediate, the HNO_2 can decompose to OH + NO via migration of a hydrogen atom. In this process the OH formed might not be excited vibrationally. Measurements of the internal-state distribution of the OH produced by the HNO + O reaction would be desirable to further understand reaction 2.

Acknowledgment. The authors wish to thank Prof. Kyle D. Bayes for his helpful suggestions and comments. Support from the Project of the Global Environment Research Program for FY 1993-1995 of Japan Environment Agency and from the Grant-in-Aid for Scientific Research on Priority Areas: Free Radical Science for FY 1993-1995 of Ministry of Education and Science is gratefully acknowledged.

References and Notes

(1) Cohen, N. *Int. J. Chem. Kinet.* **1987**, *19*, 319.

(2) Miller, J. A.; Bowman, C. T. *Prog. Energy Combust. Sci.* **1989**, *15*, 287.
(3) Dransfeld, P,; Hack, W.; Kurzke, H.; Temps, F.; Wagner, H. G. G. Twentieth Symposium (International) on Combustion; 1984, p 655.
(4) Albers, E. A.; Hoyermann, K.; Wagner, H. G. G.; Wolfrum, J. Thirteenth Symposium (international) on Combustion; 1969, p 313.
(5) Adamson, J. D.; Farhat, S. K.; Morter, C. L.; Glass, G. P.; Curl, R. F.; Phillips, L. F. *J. Phys. Chem.* **1994**, *98*, 5665.
(6) Campbell, I. M.; Handy, B. J. *J. Chem. Soc., Faraday Trans. 1*, **1975**, *71*, 2097.
(7) Tsang, W.; Herron, J. T. *J. Phys. Chem. Ref. Data*, **1991**, *20*, 609.
(8) Washida, N.; Akimoto, H.; Okuda, M. *J. Phys. Chem.* **1978**, *82*, 2293.
(9) Washida, N. *Bull. Chem. Soc. Jpn.* **1987**, *60*, 3739.
(10) Miyoshi, A.; Matsui, H.; Washida, N.*Chem. Phys. Lett.* **1989**, *160*, 291.
(11) Masaki, A.; Tsunashima, S.; Washida, N. *Chem. Phys. Lett.* **1994**, *218*, 523.
(12) Suto, M.; Lee, L. C. *J. Chem. Phys.* **1983**, *78*, 4515.
(13) Davidson, D. F.; Chang, A. Y.; Kohse-Höinghaus, K; Hanson, R. K. *J. Quantum Spectrosc. Radiat. Transfer* **1989**, *42*, 267.
(14) Baulch, D. L.; Cobos, C. J.; Cox, R. A.; Frank, P.; Hayman, G.; Just, Th.; Kerr, J. A.; Murrells, T.; Pilling, M. J.; Troe, J.; Walker, R. W.; Warnatz, J. *J. Phys. Chem. Ref. Data* **1994**, *23*, 847.
(15) DeMore, W. B.; Sander, S. P.; Golden, D. M.; Hampson, R. F.; Kulylo, M. J.; Howard, C. J.; Ravishankara, A. R.; Kolb, C. E.; Molina, M. J. *Chemical Kinetics and photochemical Data for Use in Stratospheric Modeling*, Evaluation No. 11, Publication 94-26; Jet Propulsion Laboratory: California Institute of Technology: Pasadena, CA, 1994.
(16) Diau, E. W.; Yu, T.; Wagner, M. A. G.; Lin, M. C. *J. Phys. Chem.* 1994, *98*, 4034.
(17) Quandt, R. W.; Hershberger, J. F. *J. Phys. Chem.* **1995**, *99*, 16939.
(18) Harrison, J. A.; Whyte, A. R.; Phillips, L. F. *Chem. Phys. Lett.* 1986, *129*, 346.
(19) Imamura, T.; Washida, N. *Laser Chem.* **1995**, *16*, 43.
(20) Dunlavey, S. J.; Dyke, J. M.; Jonathan, N.; Morris, A. *Mol. Phys.* **1980**, *39*, 1121.
(21) Foner, S. N.; Hudson, R. L. *J. Chem. Phys.* **1958**, *29*, 442.
(22) Kohout, F. C.; Lampe, F. W. *J. Chem. Phys.* **1966**, *45*, 1074.
(23) Chase, M. W., Jr.; Davis, C. A.; Downey, J. R., Jr.; Frurip, D. J.; McDonald, R. A.; Syverud, A. N. *J. Phys. Chem. Ref. Data* **1985**, *14*, Suppl. I.
(24) Lee, T. J.; Dateo, C. E. *J. Chem. Phys.* **1995**, *103*, 9110.
(25) Dixon, R. N. *J. Chem. Phys.* **1996**, *104*, 6905.
(26) Kutina, R. E.; Goodman, G. L.; Berkowitz, J. *J. Chem. Phys.* **1982**, *77*, 1664.
(27) Ross, S. C.; Birss, F. W.; Vervloet, M.; Ramsay, D. A. *J. Mol. Spectrosc.* **1988**, *129*, 436.
(28) (a) Donnelly, V. M.; Baronavski, A. P.; McDonald, J. R. *Chem. Phys.* **1979**, *43*, 271. (b) Donnelly, V. M.; Baronavski, A. P.; McDonald, J. R. *Chem. Phys.* **1979**, *43*, 283.
(29) Washida, N.; Bayes, K. D. *Int. J. Chem. Kinet.* **1976**, *8*, 777.
(30) Slagle, I. R.; Sarzynski, D.; Gutman, D. *J. Phys. Chem.* **1987**, *91*, 4375.
(31) Washida, N.; Martinez, R. J.; Bayes, K. D. *Z, Naturforsch.* **1974**, *29A*, 251.
(32) Timonen, R. S.; Ratajrzak, E.; Gutman, D. *J. Phys. Chem.* **1987**, *91*, 692.
(33) Yang, D. L.; Koszykowski, M. L.; Durant, Jr., J. L. *J. Chem. Phys.* **1994**, *101*, 1361.
(34) Klein, F. S.; Herron, J. T. *J. Chem. Phys.* **1964**, *41*, 1285.
(35) Ongstad, A. P.; Birks, J. W. *J. Chem. Phys.* **1986**, *85*, 3359.
(36) Sridharan, U. C.; Qiu, L. X.; Kaufman, F. *J. Phys. Chem.* **1982**, *86*, 4569.
(37) Nicovich, J. M.; Wine, P. H. *J. Phys. Chem.* **1987**, *91*, 5118.
(38) Ko, T.; Fontijn, A. *J. Phys. Chem.* **1991**, *95*, 3984.
(39) Polanyi, J. C.; Sloan, J. *Int. J. Chem. Kinet. Symp.* **1975**, *1*, 51.
(40) Spencer, J. E.; Glass, G. P. *Chem. Phys.* **1976**, *15*, 35.
(41) Silver, J. A.; Dimpfl, W. L.; Brophy, J. H.; Kinsey, J. L. *J. Chem. Phys.* **1976**, *65*, 1811.
(42) Mariella, R. P., Jr.; Lantzsch, B.; Maxson, V. T.; Luntz, A. C. *J. Chem. Phys.* **1978**, *69*, 5411.
(43) Murphy, E. J.; Brophy, J. H.; Arnold, G. S.; Dimpfl, W. L.; Kinsey, J. L. *J. Chem. Phys.* **1981**, *74*, 324.